Structural Engineering and Mechanics, Vol. 35, No. 5 (2010) 571-592
DOI: http://dx.doi.org/10.12989/sem.2010.35.5.571

A new finite element procedure for fatigue life prediction of AL6061 plates under multiaxial loadings

Wasim Tarar[1], *M.-H. Herman Shen[1], Tommy George[2] and Charles Cross[2]

[1]*Department of Aerospace Engineering, The Ohio State University, Columbus, OH 43210, USA*
[2]*Air Force Research Laboratory Wright-Patterson AFB, OH 45433, USA*

(Received February 21, 2008, Accepted February 24, 2010)

Abstract. An energy-based fatigue life prediction framework was previously developed by the authors for prediction of axial, bending and shear fatigue life at various stress ratios. The framework for the prediction of fatigue life via energy analysis was based on a new constitutive law, which states the following: the amount of energy required to fracture a material is constant. In the first part of this study, energy expressions that construct the constitutive law are equated in the form of total strain energy and the distortion energy dissipated in a fatigue cycle. The resulting equation is further evaluated to acquire the equivalent stress per cycle using energy based methodologies. The equivalent stress expressions are developed both for biaxial and multiaxial fatigue loads and are used to predict the number of cycles to failure based on previously developed prediction criterion. The equivalent stress expressions developed in this study are further used in a new finite element procedure to predict the fatigue life for two and three dimensional structures. In the second part of this study, a new Quadrilateral fatigue finite element is developed through integration of constitutive law into minimum potential energy formulation. This new QUAD-4 element is capable of simulating biaxial fatigue problems. The final output of this finite element analysis both using equivalent stress approach and using the new QUAD-4 fatigue element, is in the form of number of cycles to failure for each element on a scale in ascending or descending order. Therefore, the new finite element framework can provide the number of cycles to failure at each location in gas turbine engine structural components. In order to obtain experimental data for comparison, an Al6061-T6 plate is tested using a previously developed vibration based testing framework. The finite element analysis is performed for Al6061-T6 aluminum and the results are compared with experimental results.

Keywords: cycles; equivalent stress; energy; fatigue; finite element analysis; structures; uniaxial.

1. Introduction

Modern structural components, like gas turbine engine blades, are designed to be failure free; however, failure does occur and is commonly linked to fatigue. High cycle fatigue (HCF) is the main cause of failure in gas turbine engines (Nicholas 1999). Different design tools have been developed to analyze this issue. The most commonly used such tool is a stress versus cycles plot, or S-N curve. These curves provide fatigue strength with respect to time to failure. Other common tools for predicting fatigue properties are the Goodman diagram and the advanced Goodman

*Corresponding author, Professor, E-mail: shen.1@osu.edu

diagram (Goodman 1899), which are the popular choices for a failure-free aircraft engine design criterion. In order for designers to make an accurate assessment, the equivalent stress is calculated according to the cyclic loading conditions and compared to S-N curve or Goodman diagram to obtain the number of cycles to failure. We sometimes see: instead of uniaxial data, bench test data using components or blades also includes multiaxial results. This has led to search for a more realistic method for design comparison than the existing uniaxial design tools, which begins by observing the association between material failure/fracture and the energy dissipated during the process.

Scientists and engineers have tried since 1940's to relate energy conversion to fatigue life prediction of the material. These attempts resulted in minimal success (Feltner and Morrow 1961). The hypothesis used in this type of research implies: under cyclic loading or any bending, there exists a critical energy value for which failure occurs (Enomoto 1955). The continued research in this area later justified this hypothesis by displaying agreement between the theoretical and the experimental results on S-N curve. Further investigation of the assumption made in (Enomoto 1955) led to the introduction of a correlation between the fatigue life of a material and the strain energy dissipation during the process (Feltner and Morrow 1960, Stowell 1996). It is now understood that the strain energy required to fracture a material, monotonically, is the same as the strain energy during a cyclic fatigue procedure. Thus the critical energy value for each material is the monotonic strain energy. Based on this constitutive law, an improved energy-based criterion has been developed by the researchers to allow one to systematically determine fatigue life based on the amount of energy loss per fatigue cycle (Scott-Emuakpor *et al.* 2007, George *et al.* 2004, George *et al.* 2005, George *et al*. 2006). The previous research (Scott-Emuakpor *et al.* 2007, George *et al.* 2004, George *et al.* 2005, George *et al.* 2006) by authors includes a vibration based test method for fatigue life data acquisition and a new failure criterion. The thought behind the vibration-based methodology is supplying a dynamic base excitation to a specimen at a specified high resonant frequency, between 1200-1600 Hz, showing bending behavior. This testing method provides a significantly faster means for acquiring 10^6 cycles (between 10 & 14 minutes), therefore making it a more efficient means for acquiring HCF based on uniaxial conditions. The new failure criterion (Scott-Emuakpor *et al.* 2007) previously developed by the authors includes stress-strain relationship both for monotonic as well as cyclic loadings. This failure criterion is further used to develop fracture energy and cyclic energy expression. These expressions are used to determine the failure energy and energy dissipated per cycle. Comparison of total fracture energy to cyclic energy dissipated per cycle yields the number of cycles to failure. The other fatigue life prediction approaches in the literature are discussed in detail in (Scott-Emuakpor 2007, Tarar 2008).

In the first part of this study, the failure criterion presented in (Scott-Emuakpor *et al.* 2007) is employed in the form of strain energy in order to derive an equivalent stress expression using the distortion energy theory. The detailed formulation of this criterion is presented in section 3. The newly developed multiaxial approach is derived from the energy-based criterion and provides an opportunity to develop new fatigue finite element procedures for fatigue life analysis without accomplishing fatigue strength/life assessment through comparison with Goodman diagram or inbuilt S-N data. In this research, a new finite element procedure is proposed for multiaxial fatigue life prediction. This finite element procedure uses MSC Nastran in order to obtain the multiaxial stress state. These stresses are converted to equivalent stress using the newly developed equivalent stress expression and ultimately used to predict the number of cycles to failure. Due to the discrete nature of finite element method, the new analysis approach can provide the number of cycles to

failure for each element in the structure.

As stated earlier, the conventional approach to fatigue life prediction is based on S-N curve data, Goodman diagram or modified Goodman diagram. These tools are based on uniaxial data. Uniaxial is simply the most basic of stress states a gas turbine engine experiences and it is also the most popular experimentally due to the capability of the conventional uniaxial fatigue test machines. However, gas turbine engine components are subjected to biaxial and even multiaxial stress states due to their complex geometries and the complex interaction of aerodynamic, centrifugal, thermal, and vibratory loadings as well as fretting at interfaces and the effects of FOD. In turn, gas turbine engine components are typically designed using the Goodman Diagram which represents uniaxial test data. Therefore, engine designers must convert the biaxial or multiaxial stress states the engine components experience into equivalent uniaxial stress to utilize the Goodman diagram in their failure-free fatigue design procedure. However, fatigue failures still occur in the test and development phase of new turbine engine designs as well as high-time in-service engines in both the military and commercial fleets. There is concern in the industry that one of the reasons for these failures is that the fatigue mechanisms are different for biaxial or multiaxial stress state than they are for a uniaxial stress state. In other words, the fatigue process due to biaxial or multiaxial stress are considerably different from that of the uniaxial stress case and therefore not adequately captured by assuming an equivalent uniaxial stress. Hence, there is an increasing recognition of the need for more fatigue data under biaxial and multiaxial stress states. In order to obtain the experimental data for comparison in this study, an Al6061-T6 winger plate as shown in Fig. 1 in section 2 is tested using a previously developed vibration based fatigue testing framework (George *et al.* 2004).

In the second part of this study, the new constitutive law proposed in Scott-Emuakpor *et al.* (2007), Scott-Emuakpor (2007) are integrated into minimum potential energy formulation in order to develop a new QUAD-4 (In-Plane) fatigue element for biaxial fatigue loads. This QUAD-4 element is further modified to a QUAD-4 (Plate) element with bending capability. The procedure followed for development of this QUAD-4 element are similar to presented in Tarar *et al.* (2007) and are briefly discussed in section 5. Most research in the area of fatigue life prediction using finite element analysis is related to crack propagation (Sumi *et al.* 2005, Salvini *et al.* 1997, Fermér and Svensson 2001, Papanikos *et al.* 2003, Lee and Song 2005). The research presented in this manuscript focuses on crack initiation and provides an early insight into the fatigue failure.

Finite element analysis using equivalent stress approach as well as QUAD-4 element is performed for the winger plate shown in Fig. 1 and the results are compared to experimental results in order to validate the analysis procedure. The analysis is also performed for a curved plate, a turbine engine blade like structure, to demonstrate application of this new procedure to a real world problem.

2. Brief overview of experimental results

2.1 Specimen development

Fatigue data under biaxial or multiaxial stress is difficult and expensive to obtain using conventional machines and impossible to obtain at high frequencies. Fortunately, fully reversed bending biaxial data can be obtained using vibration based testing (George *et al.* 2004). The testing procedure provides a means of accumulating fatigue cycles on a specimen at a faster rate. It is a matter of finding a plate geometry that has a mode shape with a biaxial stress state located away

from the clamp or boundary while at the same time the von Mises stress in this biaxial stress region is at least a factor of two higher than the on von Mises stress elsewhere in the plate. This ensures the fatigue crack will develop in the desired location. Also of importance is the relative excitability of the vibration mode of interest to base excitation. This factor was not an issue for the uniaxial specimen as the two-stripe mode of the square geometry was easily excited. However, the excitability proved important for the proper design of a biaxial specimen. The modal participation factor in the plate transverse direction, or *z*-modal participation factor, is an indication of how strongly motion in the transverse or *z*-direction is represented in a particular mode shape. It is therefore a useful measure of the excitability of a particular geometry/mode to base excitation. The modal participation factors can be obtained from the data file produced by a NASTRAN free vibration analysis. The higher the value of this number, for a given geometry and mode of interest, the more likely it is that this geometry can be successfully fatigued in this mode using shaker excitation.

Various geometries were tried in order to develop the final shape suitable for producing biaxial data. The design methodology adopted for optimized design of the specimen was followed as explained in (Miyano 2003). A circular shaped geometry clamped along the circumference produces the high stresses at the desired location. However, the biaxial stress ratio for this specimen is $\sigma_y/\sigma_x = 1$ which does not meet the requirement for the suitable specimen. The other few geometries used included a combination of a rectangular and a triangulate section clamped at one end, the same section clipped at the ends, semi-diamond shaped plate and a diamond shaped plate. All these geometries complied only with one of the two desired requirements. However, they provided valuable information for evolution of the suitable shape. Ultimately, a cantilevered geometry named Winger, shown in Fig. 1 was identified as the most suitable geometry for these vibration based experiments.

The FEM analysis of the Winger geometry when constructed from 0.125" Al6061-T6 is shown in Fig. 2. Starting at the top left corner and moving clockwise, transverse displacement, von Mises stress, *y*-axis stress and *x*-axis stress are shown where *x*-direction is oriented horizontally and considered positive to the right and the *y*-direction is oriented vertically and considered positive upwards. The von Mises stress plot at the upper right of Fig. 2 shows that this geometry has significantly reduced stresses along the clamped edge in comparison with the other shapes like

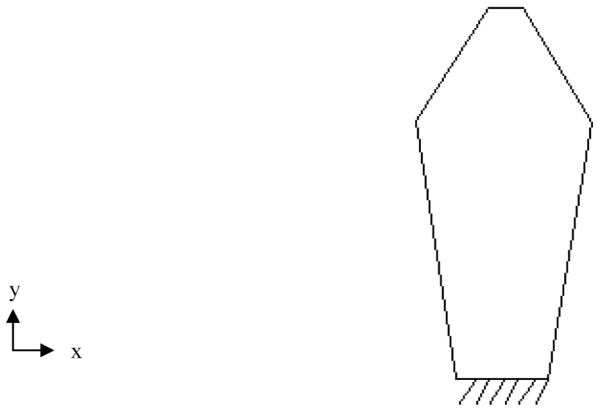

Fig. 1 Biaxial specimen winger

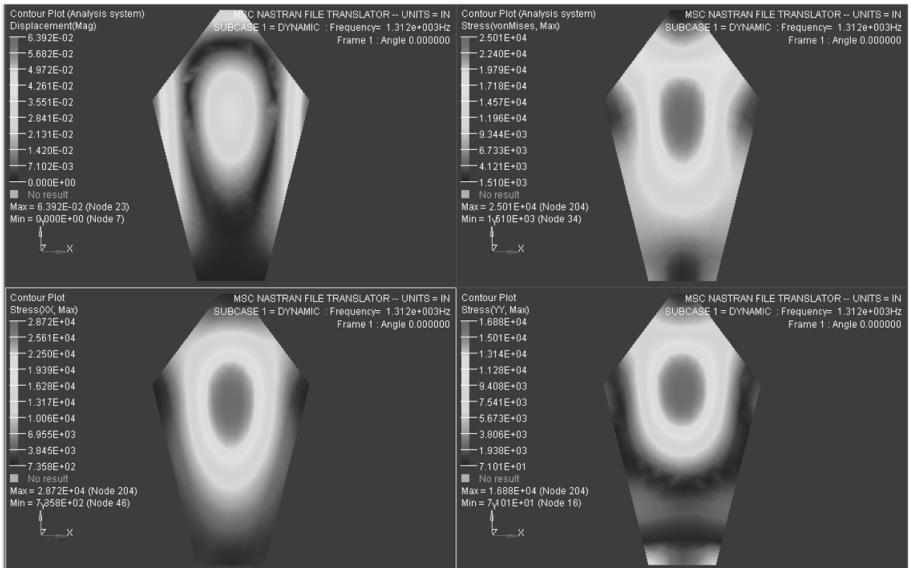

Fig. 2 FEM results (Clockwise from top left, Displacement, von-Mises, *X*-axis and *Y*-axis Stresses) for Winger Plate (0.125" thick Al6061-T6)

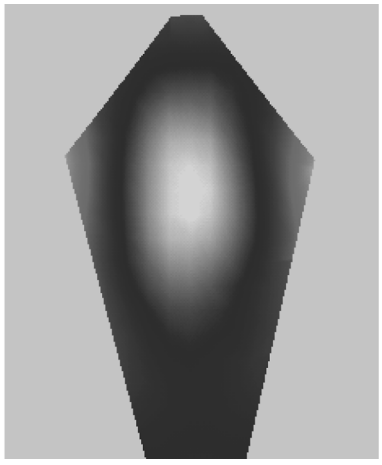

Fig. 3 Scanning laser vibrometry results of the Al 6061-T6 biaxial fatigue specimen-Mode #7 f = 1312 Hz

circular, semi-diamond, combination of rectangular and triangular geometries etc. and it is approximately a factor of 2 less than that in the fatigue region which meets our previously stated goal. A biaxial stress field with a ratio of $\sigma_Y/\sigma_X \cong 0.59$ is developed in the upper center of the plate as shown by the *x* and *y* stress plots in the lower left and right, respectively, of Fig. 2. The scanning laser vibrometry results in Fig. 3 represent mode 7 of a 0.125" thick Al6061-T6 specimen machined using the winger geometry. The vibrometry results compare favorably with the FEM mode shape in the top left quadrant of Fig. 2.

2.2 Biaxial fatigue tests

Biaxial fatigue experiments were conducted on the winger specimen made of Al6061-T6, 0.125" thick aluminum sheet. The step test method developed by Maxwell and Nicholas (2002) were used to obtain fatigue data. The stress state in the biaxial fatigue zone is either $\pm\sigma_x$ in the *X*-direction or $\pm\sigma_y$ in the *Y*-direction. Given the harmonic nature of the specimen resonant response to the sinusoidal excitation of an electrodynamic shaker, the x to y stress ratio is proportional and, like in the case of the uniaxial specimen, fully reversed or $R = -1$. To allow for comparison with uniaxial stress fatigue results the biaxial fatigue strength results are given in the form of the von Mises equivalent stress given by

$$\sigma_{equiv} = \frac{1}{\sqrt{2}}\sqrt{(\sigma_{1A}-\sigma_{2A})^2+(\sigma_{2A}-\sigma_{3A})^2+(\sigma_{3A}-\sigma_{1A})^2} \tag{1}$$

where σ_{1A}, σ_{2A}, and σ_{3A} are the principal stresses (Collins 2003). In the biaxial case in the fatigue zone of the Alumwinger3 geometry $\sigma_{3A} = 0$ and σ_{1A} and σ_{2A} are nonzero and experimentally determined from laser data calibrated to data from a delta rosette strain gage applied at the fatigue zone. The fatigue test is begun at a stress level below that of the anticipated fatigue stress, appropriate for the particular specimen material, at the number of cycles of interest. After accumulating the desired number of cycles the stress level was increased incrementally until failure occurred at which point the fatigue strength was determined using the following equation from Scott-Emuakpor *et al.* (2007), Scott-Emuakpor (2007).

$$\sigma_A = \sigma_{pr} + \frac{N_f}{10^m}(\sigma_f - \sigma_{pr}) \tag{2}$$

where in the biaxial case the stress terms in Eq. (2) are substituted with the corresponding von Mises equivalent stresses using Eq. (1). In Eq. (2), σ_A is alternative stress, σ_{pr} is alternative stress of step prior to failure in step test method, σ_f is failure stress and N_f is number of cycles to failure.

The vibration-based fatigue results at 10^6 cycles for two Al6061-T6 biaxial test specimens are given in Table 1.

The averaged von Mises equivalent stress biaxial fatigue results are compared to the previous uniaxial fatigue results average for Al6061-T6 (Scott-Emuakpor *et al.* 2007) and are presented in Table 2.

Table 2 shows that the von Mises equivalent fatigue strength results for a biaxial stress state are not consistent and significantly less than that obtained for uniaxial stress. This is typical of many

Table 1 Biaxial fatigue experimental results for Al6061-T6 for 10^6 cycles

Plate #	σ_{pr} (ksi)	σ_f (ksi)	$(\sigma_A)_{equiv}$ (ksi)
#4	15	20	18.8
#5	15	20	19.4

Table 2 Comparison of uniaxial and biaxial Al6061-T6 data for 10^6 cycles

Average Uniaxial Fatigue Strength (ksi)	26.3
Average Biaxial Von Mises Equivalent Strength (ksi)	19.1

aerospace materials and represents a significant challenge to designers who must rely on uniaxial fatigue data and indicates the need of obtaining biaxial fatigue data sets suitable for design.

3. Formulation of equivalent stress expressions

This section presents the formulation of an equivalent stress expression based on distortion energy theory. As stated in section 1, the previous research by authors (Scott-Emuakpor *et al.* 2007, George *et al.* 2004, George *et al.* 2005, George *et al.* 2006). The previous research (Scott-Emuakpor *et al.* 2007, George *et al.* 2004, George *et al.* 2005, George *et al.* 2006) includes a new failure criterion. The new failure criterion is based on the monotonic and cyclic stress-strain representation expressed by the following equations

$$\varepsilon = \frac{\sigma}{E} + \varepsilon_o \sinh\left(\frac{\sigma}{\sigma_0}\right) \tag{3}$$

$$\varepsilon = \frac{\sigma_{PP}}{E} + \frac{1}{C}\sinh\left(\frac{\sigma_{PP}}{\sigma_c}\right) \tag{4}$$

Where the parameters displayed are defined as follows: σ is the value for stress at the surface of the specimen (in the bending case, max stress), ε is the strain corresponding to the stress σ, σ_{pp} is the peak to peak stress (2σ when stress ratio is -1.0), E is the modulus of elasticity, and the variables σ_c, σ_o, ε_o, and C are curve fit parameters These curve fit parameters are obtained through statistical analysis of experimental data (Scott-Emuakpor *et al.* 2007). Eqs. (3) and (4) are used to obtain the total fracture energy and the energy dissipated per cycle. Therefore, the equations can be applied to the constitutive law to obtain the number of cycles to failure.

The above equations are further used to develop a failure energy expression. Following equation calculates total energy to failure for a monotonic case (Scott-Emuakpor *et al.* 2007).

$$W_f = \sigma_n\left(\varepsilon_n - \frac{\sigma_n}{2E}\right) + \varepsilon_o\sigma_o\left[\cosh\left(\frac{\sigma_n}{\sigma_o}\right) - 1\right] + \frac{\beta_1}{2}(\varepsilon_f^2 - \varepsilon_n^2) + \beta_o(\varepsilon_f - \varepsilon_n) \tag{5}$$

E, σ_f, and ε_f are obtained from experimental monotonic fracture results, $\varepsilon_n, \sigma_n, \beta_1$ and β_o are curve fit parameters explained in Scott-Emuakpor *et al.* (2007). The expression for cyclic energy is given by the following equation (Scott-Emuakpor *et al.* 2007).

$$W_{cycle} = \frac{2\sigma_c}{C}\left[\frac{\sigma_A}{\sigma_c}\sinh\left(\frac{2\sigma_A}{\sigma_c}\right) - \left(\cosh\left(\frac{2\sigma_A}{\sigma_c}\right) - 1\right)\right] \tag{6}$$

σ_A is the applied cyclic stress. Number of cycles to failure N is obtained through comparison of total fracture energy and energy dissipated per cycle during fatigue process (Scott-Emuakpor *et al.* 2007).

Distortion energy is stored in two parts, an energy from change in volume and energy due to the shape change. Eq. (7) displays the expression for this understanding.

$$U_T = U_v + U_D \tag{7}$$

The parameters for Eq. (7) are defined as follows: U_T is the total strain energy, U_v is the strain energy of the change in volume, and U_D is the strain energy for the change in shape.

The strain energy of the change in volume (Uv) is better known as strain energy caused by hydrostatic stress. The effect of this stress is even volumetric expansion of an infinitesimal element on all sides. The hystresis loop formed by Eq. (4) has loading and unloading curves which are a mirror image of each others. Application of this equation to cyclic loading process yields a net zero hydrostatic. Therefore during one cycle of a cyclic loading procedure, the hydrostatic stress returns to zero and the corresponding strain energy (Uv) becomes zero. In other words, only the deviatoric part of stress contributes towards failure (McClintock and Argon 1966, Scott-Emuakpor 2007). This minimizes Eq. (7) to Eq. (8) and shows that the total energy within a hysteresis loop is purely distortion energy.

$$U_T = U_D \tag{8}$$

Furthermore, if it can be justified that the total monotonic strain energy density of a volume subjected to multi-axial loading is the summation of the six areas under the curves formed by the respective stress-strain relationships, it can then be implied that the total strain energy density in one multi-axial cycle is the summation of the directional (3 for Principle-axes and 6 for Cartesian-axes) hysteresis loops acting on the volume. Therefore to acquire an equivalent stress value from Eq. (8), this implication is displayed for principle axes by Eq. (9): where ε_E and ε_i are functions of stress shown by Eqs. (13) and (14) respectively, $\sigma_{pp,E}$ and $\sigma_{PP,i}$ are the generalized stress values corresponding to the generalized cyclic strains ε_E and ε_i (i.e., the minimum fully reversed point is observed as the origin), and i denotes the principle direction, which are values from 1-3.

$$\sigma_{PP,E}\varepsilon_E - 2\int_0^{\sigma_{PP,E}} \varepsilon_E d\sigma_{PP,E} = \sum_{i=1}^{3} \sigma_{PP,i}\varepsilon_i - 2\int_0^{\sigma_{PP,i}} \varepsilon_i d\sigma_{PP,i} \tag{9}$$

Eq. (9) can further be modified to include the Poisson's ratio effect using Hook's Law relations given below (Chandraputla and Belegunda 2002).

$$\varepsilon_1 = \frac{1}{E}[\sigma_1 - \nu(\sigma_2 + \sigma_3)] \tag{10}$$

$$\varepsilon_2 = \frac{1}{E}[\sigma_2 - \nu(\sigma_1 + \sigma_3)] \tag{11}$$

$$\varepsilon_3 = \frac{1}{E}[\sigma_3 - \nu(\sigma_1 + \sigma_2)] \tag{12}$$

Proceeding evaluation of Eq. (9) and including the Poisson's ratio effect, the expression for Eq. (13) is acquired.

$$\frac{\sigma_{PP,E}}{C}\sinh\left(\frac{\sigma_{PP,E}}{\sigma_c}\right) - \frac{\sigma_c}{C}\int_0^{\sigma_{PP,E}} \sinh\left(\frac{\sigma_{PP,E}}{\sigma_c}\right) d\sigma_{PP,E} = A - B \tag{13}$$

where

$$A = \sum_{i=1}^{3} \frac{1}{C}[A1 - \nu(A2 + A3)] \quad \text{and}$$

$$A1 = \sigma_{PP,i}\sinh\left(\frac{\sigma_{PP,i}}{\sigma_c}\right), \quad A2 = \sigma_{PP,j}\sinh\left(\frac{\sigma_{PP,j}}{\sigma_c}\right), \quad A3 = \sigma_{PP,k}\sinh\left(\frac{\sigma_{PP,k}}{\sigma_c}\right)$$

and

$$B = \sum_{i=1}^{3} \frac{2}{C}[B1 - v(B2 + B3)]$$

where

$$B1 = \int_0^{\sigma_{PP,i}} \sinh\left(\frac{\sigma_{PP,i}}{\sigma_c}\right) d\sigma_{PP,i}, \quad B2 = \int_0^{\sigma_{PP,j}} \sinh\left(\frac{\sigma_{PP,j}}{\sigma_c}\right) d\sigma_{PP,j}, \quad B3 = \int_0^{\sigma_{PP,k}} \sinh\left(\frac{\sigma_{PP,k}}{\sigma_c}\right) d\sigma_{PP,k}$$

and

$i = 1, 2, 3$
$j = 2, k = 3,$ if $i = 1$
$j = 1, k = 3,$ if $i = 2$
$j = 1, k = 2,$ if $i = 3$

To simplify this expression for use in determination of equivalent stress, the summation of the integrated expression on the right side of Eq. (13) is assumed to be equal to the integrated portion of the equivalent stress calculation on the left side. Therefore, following integration of both sides and replacing hyperbolic trigonometry with exponential functions, the expression in Eq. (14) is acquired.

$$e^{\frac{2\sigma_E}{\sigma_c}} + e^{-\frac{2\sigma_E}{\sigma_c}} + 1 = \sum_{i=1}^{3} \left(e^{\frac{2}{\sigma_c}(\sigma_i - v(\sigma_j + \sigma_k))} + e^{-\frac{2}{\sigma_c}(\sigma_i - v(\sigma_j + \sigma_k))} + 1 \right) \tag{14}$$

Upon further analysis of Eq. (14), two assumptions are made: (1) the numerical portion has a minimal effect in the equation, and the exponential functions of similar signs on both sides of the equation are equivalent. In other words, Eq. (15) is assumed to be a true expression.

$$e^{\frac{2\sigma_E}{\sigma_c}} = \sum_{i=1}^{3} \left(e^{\frac{2}{\sigma_c}(\sigma_i - v(\sigma_j + \sigma_k))} \right) \tag{15}$$

The resulting expression for calculating equivalent stress using the energy-based methodology is displayed by Eq. (16).

$$\sigma_E = \frac{\sigma_c}{2} \ln\left(\sum_{i=1}^{3} e^{\frac{2}{\sigma_c}(\sigma_i - v(\sigma_j + \sigma_k))} \right) \tag{16}$$

The number of cycles to failure can be acquired by inserting the equivalent stress expression into Eqs. (5) and (6).

$$N = C \frac{\sigma_n\left(\varepsilon_n - \frac{\sigma_n}{2E}\right) + \varepsilon_O \sigma_O \left[\cosh\left(\frac{\sigma_n}{\sigma_O}\right) - 1\right] + \frac{\beta_1}{2}(\varepsilon_f^2 - \varepsilon_n^2) + \beta_O(\varepsilon_f - \varepsilon_n)}{2\sigma_c \left\{ \frac{\sigma_E}{\sigma_c} \sinh\left(\frac{2\sigma_E}{\sigma_c}\right) - \left[\cosh\left(\frac{2\sigma_E}{\sigma_c}\right) - 1\right] \right\}} \tag{17}$$

4. Finite element procedures

4.1 Equivalent stress approach

A traditional HCF turbine blading system design procedure based on conventional fatigue life prediction approach is shown schematically in Fig. 4. This design process usually consists of a structural dynamics analysis to determine natural frequencies and mode shapes at certain operating speed ranges and a stress analysis using a finite element based tool such as MSC NASTRAN and ANSYS (LMS Engineering Innovations: http://www.lmsintl.com, Desktop Engineering (DE): http://www.deskeng.com, MSC Software: http://www.mscsoftware.com) to calculate the dynamic stress distribution for identifying the maximum vibratory stress location or area under a series of given excitations. Once the maximum stresses for each vibration mode are determined, high cycle fatigue assessment can be achieved by measuring the margin between the maximum vibratory stress and the material fatigue capability which is a straight line drawn between the mean ultimate strength at zero vibratory stress and mean fatigue strength at 10^7 cycles (or infinite life). A typical Goodman

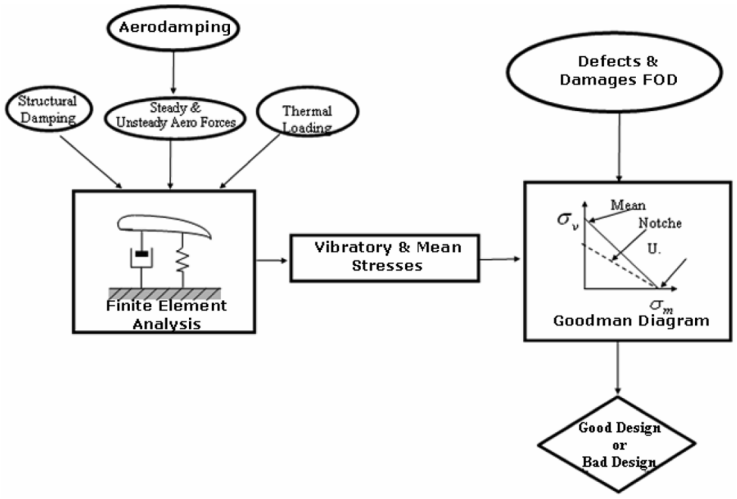

Fig. 4 Conventional finite element analysis approach to fatigue life prediction

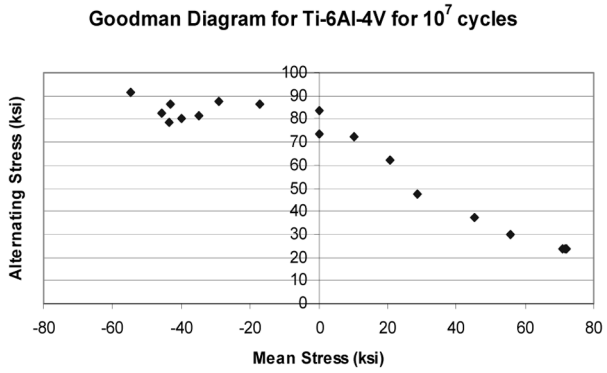

Fig. 5 Typical Goodman (or Haigh) Diagram for Ti-6Al-4V for 10^7 cycles

diagram for the titanium alloy Ti-6Al-4V is shown in Fig. 5 (Miyano 2003), constructed using uniaxial fatigue data.

The Finite element procedure for this research consists of performing a free vibration analysis using MSC NASTRAN in order to identify the suitable natural mode for excitation. The requirements for selection of suitable mode are the same as stated in section 2 while selecting the suitable geometry for experiments. The next step is to excite the identified mode through frequency response finite element analysis in MSC NASTRAN and obtain the vibratory stresses for each element present at various locations in the structure. These stresses are converted to equivalent stress using newly developed equivalent stress expression in Eq. (16). Finally, the number of cycles to failure is obtained from Eq. (17) providing fatigue life for every location in the structure. The analysis generates two kinds of output files. The text format output file contains number of cycles to failure data for each element in the structure. The binary output file contains failure cycles data which is plotted in the form of colored contour where different colors represent the respective fatigue life for the structure. In this finite element analysis procedure, Altair Hypermesh is used for preprocessing, MSC NASTRAN is used as a finite element solver, Altair Hyperview and Matlab are used as postprocessors.

The biaxial fatigue experimental results generated for an Al6061-T6 winger plate are already discussed in section 2. A finite element model of this plate is shown in Fig. 6.

As discussed in section 2, the free vibration analysis of Winger plate is performed and mode 7 is identified as the appropriate mode for this analysis. In next step, the forced response analysis is performed and vibratory stresses are obtained for the same mode at the respective frequency. These stresses are converted to equivalent stress and ultimately to number of cycles to failure for the Winger plate. The results from this analysis are presented in the following section. These fatigue life results are compared to experimental results presented in section 2 for biaxial fatigue life for AL6061-T6.

In order to apply this new approach to more real world applications, a turbine engine blade like curved plate structure is also analyzed. The profile, geometry and a finite element model of this curved plate are shown in the following figures.

The finite element analysis results for curved plate are presented in the Results and Discussion section.

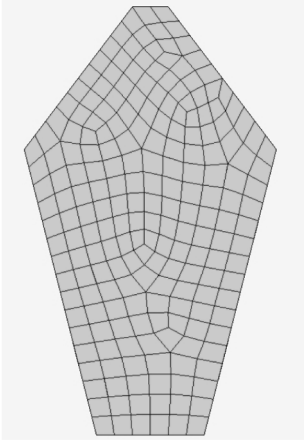

Fig. 6 A finite element mesh for Al6061-T6 Winger Plate

Fig. 7 Outer profile of curved plate (Al6061-T6)

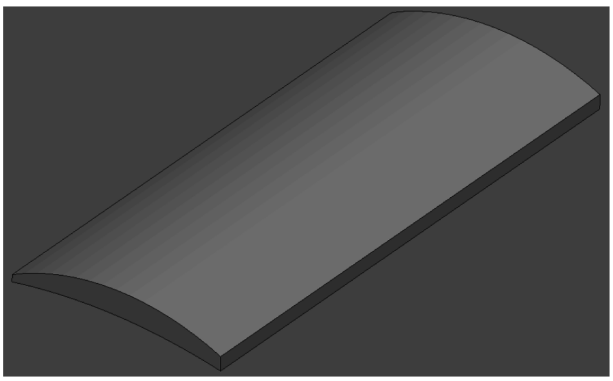

Fig. 8 Geometry of curved plate (Al6061-T6)

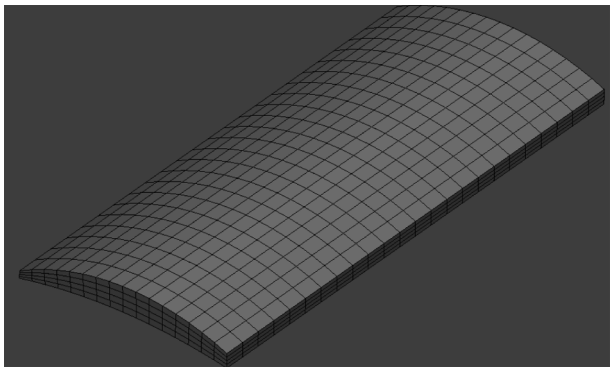

Fig. 9 A finite element mesh of curved plate (Al6061-T6)

4.2 Development of new quad-4 fatigue elemente

The procedures followed for development of new QUAD-4 element are similar to presented by authors in (Tarar *et al.* 2007) for development of uniaxail rod fatigue element.

The uniaxail constitutive law both for monotonic as well as cyclic loading are represented by Eqs. (3) and (4) (Scott-Emuakpor *et al.* 2007). The following equations represent stress-strain relationships for shear monotonic and cyclic loads respectively (Scott-Emuakpor 2007).

$$\gamma_{monotonic} = \frac{\tau}{G} + \gamma_O \sinh\left(\frac{\tau}{\tau_O}\right) \tag{18}$$

$$\gamma_{cyclic} = \frac{\tau_{PP}}{G} + \frac{1}{C_S} \sinh\left(\frac{\tau_{PP}}{\tau_c}\right) \tag{19}$$

where the parameters displayed in above equations are defined as follows: γ is the strain corresponding to τ, τ_{pp} is the peak to peak stress, G is the modulus of shear, and the variables τ_c, τ_o, γ_o and C_s are curve fit parameters (Scott-Emuakpor 2007).

As is evident from Eqs. (3), (4), (18) and (19), the stress-strain relationship consists of two parts: linear elastic and a non-linear plastic expression. Integration of elastic part into minimum potential energy formulation is a classical finite element problem and is available in literature (Reddy 1984, Chandraputla and Belegunda 2002). Integration of non-linear parts of constitutive law is presented below.

If a two dimensional (2-D) stress tensor is defined as following

$$\{\sigma_{ij}\} = \begin{bmatrix} \sigma_{xx} & \tau_{xy} \\ \tau_{yx} & \sigma_{yy} \end{bmatrix} \tag{20}$$

The corresponding stress elements for plastic part of Eqs. (3), (4), (18) and (19) are given by the following equations.

$$\sigma_{pm-xx} = \sigma_0 \sinh^{-1}\left(\frac{\varepsilon_{px}}{\varepsilon_0}\right) \tag{21}$$

$$\sigma_{pm-yy} = \sigma_0 \sinh^{-1}\left(\frac{\varepsilon_{py}}{\varepsilon_0}\right) \tag{22}$$

$$\sigma_{pm-xy} = \tau_0 \sinh^{-1}\left(\frac{\gamma_{pxy}}{\gamma_0}\right) \tag{23}$$

The subscripts *pm* designate the plastic case for monotonic loading.

A four-node QUAD element is shown in the following figure. The element has four nodes with each node having two degrees of freedom, displacements in x and y directions.

d denotes the modal displacement vector and d_s are x and y displacements at each node. The displacement at any point within the element is denoted by $u = [u(x, y), v(x, y)]^T$.

$$d = [d_1, d_2, d_3, d_4, d_5, d_6, d_7, d_8]^T \tag{24}$$

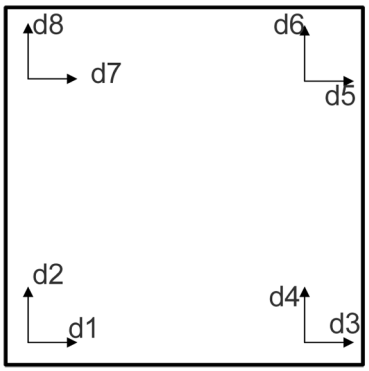

Fig. 10 A four Node QUAD Element

As stated earlier, the procedure followed for development of new QUAD-4 fatigue element are similar to presented by the authors in (Tarar *et al.* 2007). The QUAD-4 element shown in Fig. 10 is represented in natural coordinates ($\xi - \eta$) and Lagrange shape functions are used to approximate the element.

Integration of Eq. (20) into Eq. (25) provides new K-matrix for the plastic part of the constitutive law fatigue analysis.

$$\Pi = \int \sigma^T \varepsilon dV - \int u f dV - \int u T dx - \sum u_i P_i \tag{25}$$

Where Π is the minimum potential energy, σ is the stress tensor, ε is the strain vector, u is the displacement, f is the body force, T is the traction force, and P_i is the point load. V is the volume and x denotes the length of the element.

The QUAD-4 K-Matrices for linear elastic and non-linear plastic parts are represented by the following equations.

$$K_{em-Plane} = \int_{-1}^{1}\int_{-1}^{1} [k_{ij}] d\xi d\eta \quad \text{for } i = 0 \ldots\ldots 8 \text{ and } j = 0 \ldots\ldots 8 \tag{26}$$

$$K_{pm-Plane} = \int_{-1}^{1}\int_{-1}^{1} [k_{ijpm}(d)] d\xi d\eta \quad \text{for } i = 0 \ldots\ldots 8 \text{ and } j = 0 \ldots\ldots 8 \tag{27}$$

Where subscripts *em* and *pm* denote the elastic and plastic cases respectively.

The elements of $K_{pm\text{-}Plane}$ are given in the following equations

$$k_{ij-pm} = \frac{1}{4}\left[\frac{Q_i s_{ij} Q_j}{R_{11}}\right] \quad \text{for} \quad i = 1, 3, 5, 7 \text{ and } j = 1, 3, 5, 7 \tag{28}$$

$$k_{ij-pm} = \frac{1}{4}\left[\frac{Q_i s_{ij} Q_j}{R_{12}}\right] \quad \text{for} \quad i = 1, 3, 5, 7 \text{ and } j = 2, 4, 6, 8 \tag{29}$$

$$k_{ij-pm} = \frac{1}{4}\left[\frac{Q_i s_{ij} Q_j}{R_{12}}\right] \quad \text{for} \quad i = 2, 4, 6, 8 \text{ and } j = 2, 4, 6, 8 \tag{30}$$

$$k_{ij-pm} = \frac{1}{4}\left[\frac{Q_i s_{ij} Q_j}{R_{11}}\right] \quad \text{for} \quad i = 2, 4, 6, 8 \text{ and } j = 1, 3, 5, 7 \tag{31}$$

where Q_i, Q_j, S_{ij}, R_{11} and R_{12} are given by the following Table.

L and W are length and width of the element respectively. The similar equations are developed for cyclic loads. The resulting K-matrices are shown in Eqs. (32) and (33).

$$K_{ec-Plane} = \int_{-1}^{1}\int_{-1}^{1} [k_{ij}] d\xi d\eta \quad \text{for } i = 0 \ldots\ldots 8 \text{ and } j = 0 \ldots\ldots 8 \tag{32}$$

$$K_{pc-Plane} = \int_{-1}^{1}\int_{-1}^{1} [k_{ijpc}(d)] d\xi d\eta \quad \text{for } i = 0 \ldots\ldots 8 \text{ and } j = 0 \ldots\ldots 8 \tag{33}$$

The elements of $K_{pc\text{-}Plane}$ are the same as given in Eqs. (28) to (31) except that the parameters σ_o

Table 3 Constants for Eqs. (28) to (31)

i/j	$Q_{i/j}$	S_{ij}	R_{11} and R_{12}
1	$-\frac{W}{2}(1-\eta)$	$S_{ij} = \sigma_0 \sinh^{-1}\left(\frac{\varepsilon_{px}}{\varepsilon_0}\right)$ for $i = 1, 3, 5, 7$ and $j = 1, 3, 5, 7$	$R_{11} = \frac{W}{2}\left(\begin{matrix} -d1 + d3 + d5 - d7 \\ + (d1 - d3 + d5 - d7)\eta \end{matrix}\right)$
2	$-\frac{L}{2}(1-\xi)$		
3	$\frac{W}{2}(1-\eta)$	$s_{ij} = \sigma_0 \sinh^{-1}\left(\frac{\varepsilon_{py}}{\varepsilon_0}\right)$ for $i = 2, 4, 6, 8$ and $j = 2, 4, 6, 8$	
4	$-\frac{L}{2}(1+\xi)$		
5	$\frac{W}{2}(1+\eta)$	$S_{ij} = \tau_0 \sinh^{-1}\left(\frac{\gamma_{pxy}}{\gamma_0}\right)$ for $i = 2, 4, 6, 8$ and $j = 1, 3, 5, 7$	$R_{12} = \frac{L}{2}\left(\begin{matrix} -d2 - d4 + d6 + d8 \\ + (d2 - d4 + d6 - d8)\xi \end{matrix}\right)$
6	$\frac{L}{2}(1+\xi)$		
7	$-\frac{W}{2}(1+\eta)$	$S_{ij} = \tau_0 \sinh^{-1}\left(\frac{\gamma_{pxy}}{\gamma_0}\right)$ for $i = 1, 3, 5, 7$ and $j = 2, 4, 6, 8$	
8	$\frac{L}{2}(1-\xi)$		

changes to σ_c, ε_o changes to $1/C$, τ_o changes to τ_c, γ_o changes to $1/Cs$ and the applied stress σ and τ changes to peak to peak stress σ_{PP} and τ_{PP}.

Eqs. (27) and (33) are non-linear due to presence of "*ds*" in the resulting K-matrices. To account for the non-linear behavior, the Newton-Raphson iteration method is applied to the analysis (Khurram and Masud 2006, Masud and Khurram 2004, Reddy 2004). These K-matrices are used in Eq. (34) to determine the unknown degrees of freedom.

$$[K]\{d\} = \{F\} \tag{34}$$

The loads are applied from 0 to peak to peak. The results are post-processed using classical FEA techniques. The nodal displacement results are further used to obtain stresses and strains for each element in the structure. The 2-D stresses and strains are converted to equivalent von-Mises stress and strain. These stresses and strains are used to calculate the energy dissipated per cycle and ultimately the number of cycles to failure for each element. The calculations of energy and postprocessing procedures are the same as (Tarar *et al.* 2007) for development of uniaxail rod fatigue element.

In order to verify the QUAD-4 element, this element is benchmarked against a uniaxial rod element developed in (Tarar *et al.* 2007). A 2-D plate is meshed with the new QUAD-4 elements and subjected to uniaxial tension in *x*-direction in the form of displacement. The displacement solution is compared to the solution of a 1-D bar meshed with the rod element and subjected to uniaxial tension. The plate and rod are fixed at left end/side and a unit displacement is applied at

the right most end of rod and right most edge of plate. The linear QUAD-4 Fatigue K-matrix results are compared to the linear 1-D rod solution as well as an ANSYS solution of the same problem.

As stated earlier, the non-linear analysis requires an iterative approach. The non-linear QUAD-4 Fatigue K-matrix results are compared to the linear 1-D rod solution. The results for non-linear analysis are shown in the following figure and a comparison is made in the following table.

As is evident from the results of Fig. 12 and Table 4, the QUAD-4 fatigue element analysis compares exactly with the 1-D rod fatigue element. These results successfully complete the benchmarking of the new QUAD-4 fatigue.

In order to develop QUAD-4 fatigue element with bending capability, the QUAD-4 (In-plane) element is modified to have additional degrees of freedom per node to include rotation and bending as well. This modification is shown in the following figure.

The new QUAD-4 element is used to model the Winger Plate and the results are compared to experimental data and equivalent stress approach prediction. In order to have a closer comparison,

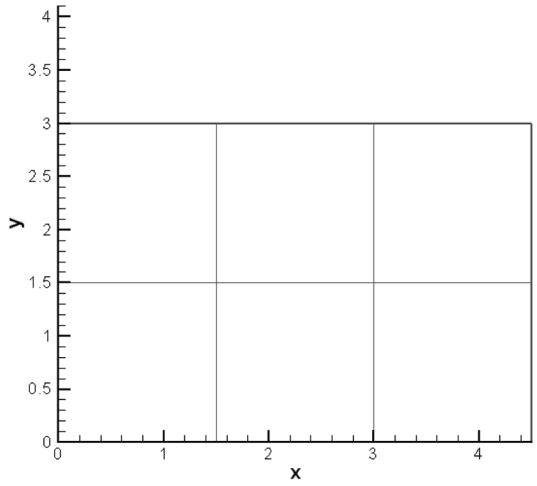

Fig. 11 6-element mesh for 2-D plate

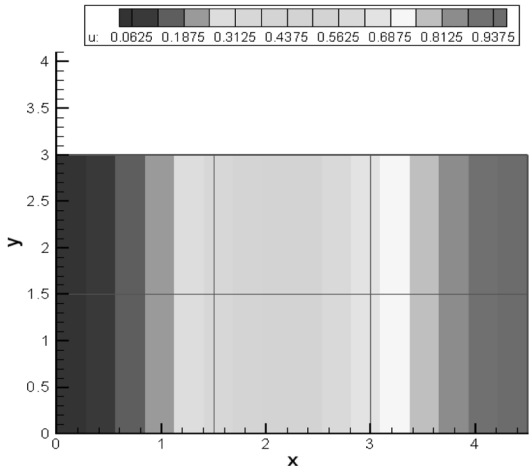

Fig. 12 Displacement results using non-linear QUAD-4 fatigue element

Table 4 Non-linear analysis benchmarking of QUAD-4 element

Iteration No.	Node 2		Node 3		Node 4	
	Non-Linear Axial	Non-Linear 2D QUAD-4	Non-Linear Axial	Non-Linear 2D QUAD-4	Non-Linear Axial	Non-Linear 2D QUAD-4
1	0.0636458	0.0636469	0.1351291	0.1351315	1.0000	1.0000
2	0.0815309	0.0815353	0.1731019	0.1731112		
5	0.1003474	0.1003337	0.2130519	0.2130229		
9	0.1102611	0.1102664	0.2341001	0.2341113		
10	0.1182828	0.1182878	0.2511314	0.2511419		
12	0.1277408	0.1277448	0.2712119	0.2712204		
35	0.2125675	0.2125580	0.4513112	0.4512910		
49	0.3333354	0.3333794	0.6666702	0.6665912		

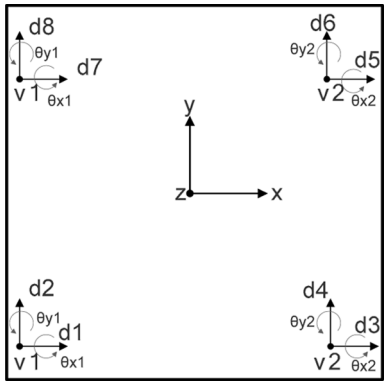

Fig. 13 QUAD-4 plate element obtained by addition of modified beam element and QUAD-4 plane element

Winger plate meshed with new plate element is excited to stress level of 25 ksi for 7th mode and the stress and prediction results are compared to the equivalent stress approach prediction. Eq. (34) is modified for this analysis into a dynamic analysis (Meirovitch 2002) as given by Eq. (35).

$$[M]\{\ddot{d}\} + [K]\{d\} = \{F\cos\omega t\} \tag{35}$$

where M is the mass matrix and ω is the frequency. The results are presented in Results and Discussion section.

5. Results and discussion

5.1 Equivalent stress approach

Fig. 14 shows mode shape 7 for Winger Plate. The results are obtained from MSC NASTRAN free vibration finite element analysis.

Fig. 15 shows the vibratory stress results from the MSC NASTRAN forced response finite element analysis results. The Winger Plate has been excited to a maximum stress level of 25 ksi.

The fatigue results for Winger plate are shown in Fig. 16. The cycles are plotted on a reverse scale with minimum cycles shown at the top of the scale in red color and the maximum cycles at the bottom of the scale in blue color. The high stresses in the winger plate are concentrated away from the fixed end as shown in Fig. 15. Therefore, the low cycles is also observed in the same area. Table 5 shows the comparison of experimental and finite element analysis results for Al6061-T6 for 10^6 cycles. These results are obtained from the text output file generated by the analysis. The FEA fatigue life predictions compare well with the experimental results thus validating the newly developed equivalent stress expression and the new analysis approach.

Fig. 17 shows the desired mode shape for the curved plate previously discussed in section 4.

The vibratory stress results are shown in Fig. 18. The stresses are concentrated in the area away from the fixed end of the plate.

Fig. 20 shows the fatigue prediction results from the finite element analysis of the curved plate. The low cycles are observed in the same area where the maximum stresses are present.

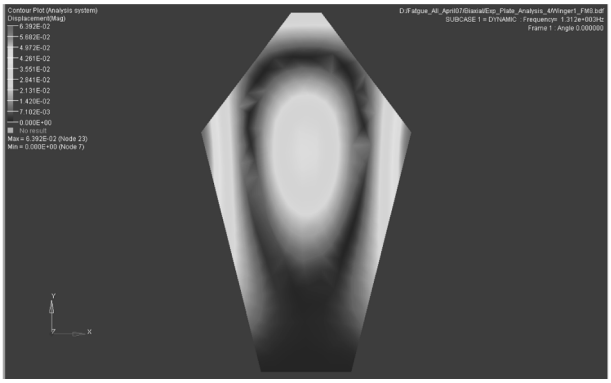

Fig. 14 Displacement (Mode #7, Frequency=1312 Hz) results for Winger Plate (Al6061-T6)

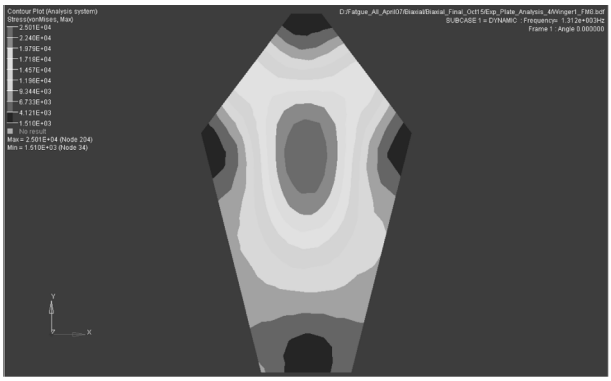

Fig. 15 Vibratory stress results for Winger Plate (Al6061-T6)

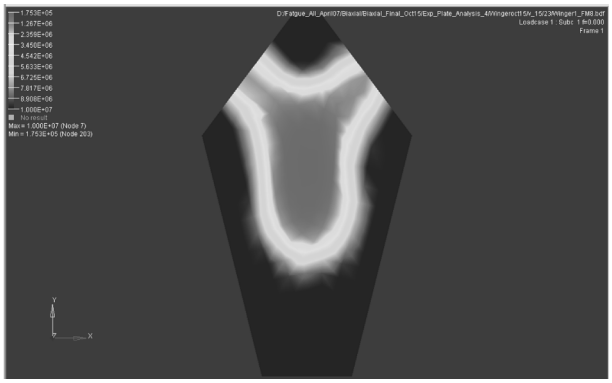

Fig. 16 Numbers of cycle to failure results for Winger Plate (Al6061-T6)

Table 5 Biaxial fatigue results for Al6061-T6 for 10^6 cycles

	Stress (ksi)	Experiment Life Cycles	FE Analysis Life Cycles
Winger Plate	19.1	10^6	1.26×10^6

5.2 QUAD-4 analysis results

The following figure shows the stress results for a Winger plate analyzed using new QUAD-4 (Plate) element.

The following Table shows a comparison of results from vibration analysis performed on Winger plate meshed with new QUAD-4 (Plate) element. The results match well with the experimental

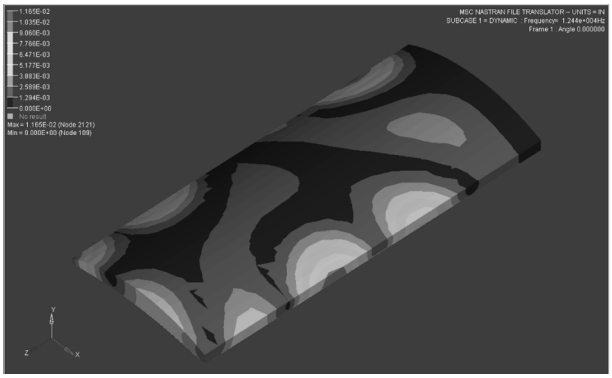

Fig. 17 Displacement (Frequency = 12444 Hz) results for curved plate (Al6061-T6)

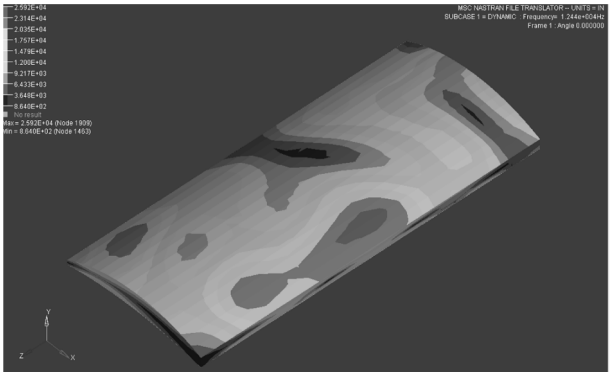

Fig. 18 Vibratory stress results for curved plate (Al6061-T6)

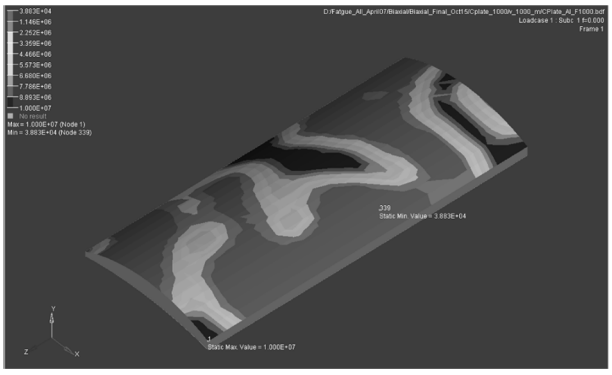

Fig. 19 Numbers of cycle results for curved plate (Al6061-T6)

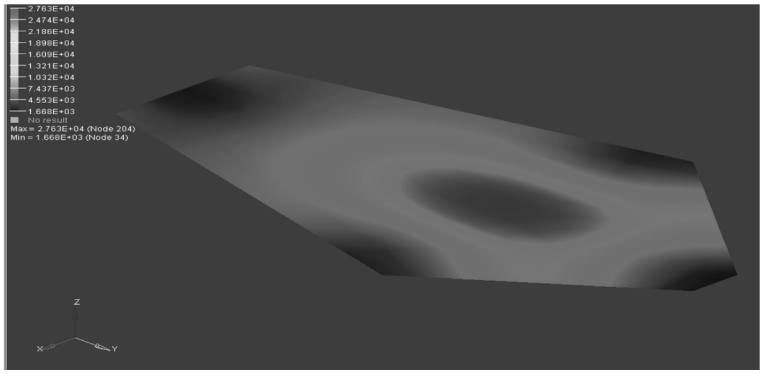

Fig. 20 7th mode stress results (QUAD-4 (Plate) element)

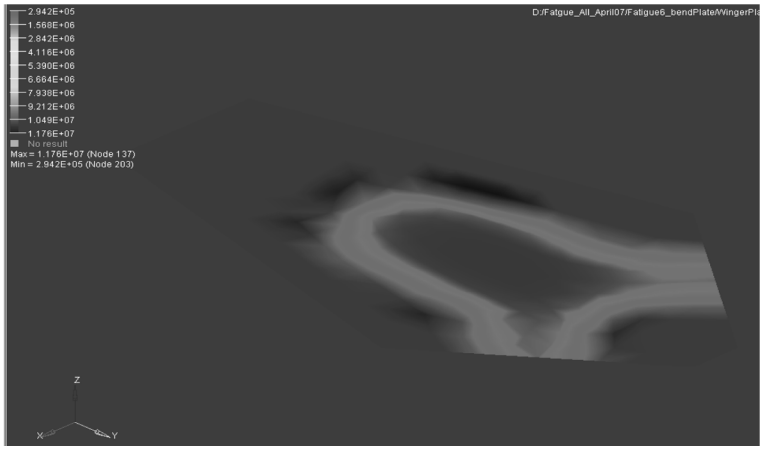

Fig. 21 Fatigue life prediction (QUAD-4 (Plate) element)

Table 6 Comparison of plate element results with experimental and equivalent stress approach

	Stress (ksi)	Experiment Life Cycles	FE Analysis Equivalent Stress Approach	FE Analysis QUAD-4 (Plate) Element
Winger Plate	19.1	10^6	1.26 × E6	1.16 × E6

results as well as the equivalent stress approach discussed in previous sections.

The equivalent stress fatigue analysis presented in this research follows part of the conventional analysis approach (MSC Software, LMS Engineering Innovations, Desktop Engineering (DE)) as it obtains the stresses through dynamic analysis using ordinary QUAD-4 elements. When performing the analysis with new QUAD-4 element, the mode shapes and stresses are obtained from direct analysis of the component meshed with the QUAD-4 fatigue elements. Therefore, this analysis in comparison to equivalent stress approach skips multiple analysis steps and makes the prediction one step analysis. Furthermore, the prediction results with QUAD-4 fatigue elements show closer comparison to experimental results as compared to the equivalent stress approach. The new QUAD-4 elements developed in this research predict crack initiation whereas most research in this area

(Sumi *et al.* 2005, Salvini *et al.* 1997, Fermér and Svensson 2001, Papanikos *et al.* 2003, Lee and Song 2005) is related to crack propagation.

6. Conclusions

The need for generating a biaxial fatigue data for biaxial loads is well demonstrated through experiments. The development of the equivalent stress expression based on an improved fatigue life prediction criterion and application of this new expression in a finite element procedure provides a useful tool for fatigue life prediction in gas turbine engine structural components. The prediction of number of cycles with the new finite element procedure and a comparison of results to experimental data signifies that the new finite element procedure provides encouraging estimation of number of cycles for biaxial fatigue loading. The equivalent stress expression developed in this research is applicable to multiaxial fatigue as well. Therefore, the finite element procedure applied to biaxial fatigue can easily be extended to multiaxial fatigue process. However, this requires a generation of multiaxial experimental fatigue data in order to validate the results. The capability of this new approach to predict fatigue life for each location in the gas turbine engine structural component provides a complete visual picture of the fatiguing process in the component.

The results presented in section 5.2 and comparison of these results to experimental data and equivalent stress approach show that new QUAD-4 elements can predict the fatigue life of structural component with sufficient accuracy. As these elements are developed from energy-based constitutive law for fatigue life prediction, therefore, analysis with these elements incorporates the fatigue mechanism into fatigue analysis. Due to the discrete nature of finite element analysis, new fatigue elements can predict number of cycles to failure at each location in the 2-D structures.

Acknowledgements

The authors would like to thank the Air Force Research Laboratory, Propulsion Directorate at Wright-Patterson Air Force Base, Ohio for their financial support and encouragement of this research.

References

Chandraputla, T.R. and Belegunda, A.D. (2002), *Introduction to Finite Elements in Engineering*, Prentice-Hall, Inc.

Collins, J.A. (2003), *Mechanical Design of Machine Elements and Machines*, John Willey and Sons.

Desktop Engineering (DE), http://www.deskeng.com

Enomoto, N. (1955), "On fatigue tests under progressive stress", *Proc. Am. Soc. Test. Mater.*, **55**, 903-917.

Feltner, C.E. and Morrow, J.D. (1961), "Micro plastic strain hysteresis energy as a criterion for fatigue facture", *J. Basic Eng., Tran. ASME*, **83**, 15-22.

Fermér, M. and Svensson, H. (2001), "Industrial experiences of FE-based fatigue life predictions of welded automotive structures", *Fatigue Fract. Eng. M.,* **24**(7), 489-500.

George, T., Seidt, J., Shen, M.H.H., Cross, C. and Nicholas, T. (2004), "Development of a novel vibration-based fatigue testing methodology", *Int. J. Fatigue*, **26**(5), 477-486.

George, T., Shen, M.H.H., Cross, C. and Nicholas, T. (2006), "A new multiaxial fatigue testing method for variable-amplitude loading and stress ratio", *J. Eng. Gas Turb. Power*, **128**, 857-864.
George, T., Shen, M.H.H., Scott-Emuakpor, O., Cross, C., Nicholas, T. and Calcaterra, J. (2005), "Goodman diagram via vibration-based fatigue testing", *J. Eng. Mater. Technol*., **127**(1), 58-64.
Goodman, J. (1899), *Mechanics Applied to Engineering,* Longmans, Green and Co., London.
Khurram, R.A. and Masud, A. (2006), "A multiscale/stablized formulation of the incompressible navier-stokes equations for moving boundary flows and fluid structure interaction", *Comput. Mech.*, **38**, 4-5.
Lee, H.J. and Song, J.H. (2005), "Finite-element analysis of fatigue crack closure under plane strain conditions: stabilization behavior and mesh size effect", *Fatigue Fract. Eng. M.,* **28**(3), 333-342.
LMS Engineering Innovations, http://www.lmsintl.com
Masud, A. and Khurram, R.A. (2004), "Multiscale finite element method for the incompressible navier-stokes equations", *Comput. Meth. Appl. Mech. Eng.,* **193**, 21-22.
McClintock, F.A. and Argon, A.S. (1966), *Mechanical Behavior of Material*, Addison Wesley.
Meirovitch, L. (2001), *Fundamentals of Vibration*, McGraw-Hill Company, New York.
Miyano, T. (2003), "High cycle fatigue specimen topology design", MS Thesis, The Ohio State University.
MSC Software, http://www.mscsoftware.com
Nicholas, T. (1999), "Critical issues in high cycles fatigue", *Int. J. Fatigue*, **21**, 221-231.
Nicholas, T. and Maxwell, D. (2002), "Mean stress effects on the high cycle fatigue limit stress in Ti-6Al-4V", *Fatigue Fract. Mech*., ASTM STP 1417, **33**, 476-492.
Papanikos, P., Tserpes, K.I. and Pantelakis, S.P. (2003), "Modeling of fatigue damage progression and life of CFRP laminates", *Fatigue Fract. Eng. M.,* **26**(1), 37-47.
Reddy, J.N. (1984), *An Introduction to the Finite Element Methods*, McGraw-Hill Book Company, New York.
Reddy, J.N. (2004), *An Introduction to Non-Linear Finite Element Analysis*, Oxford University Press, New York.
Salvini, P., Cardecchhia, E. and Emofonti, G. (1997), "A procedure for fatigue life prediction of spot welded joints", *Fatigue Fract. Eng. M.,* **20**(8), 1117-1128.
Scott-Emuakpor, O. (2007), "Development of a noval energy based method for multiaxial fatigue strength assessment", Graduate Program of Mechanical Engineering, The Ohio State University.
Scott-Emuakpor, O., Shen, M.H.H., Cross, C., Calcaterra, J. and George, T. (2007), "Development of an improved high cycle fatigue criterion", *J. Eng. Gas Turb. Power*, **129**, 162-169.
Stowell, E. (1996), "A study of the energy criterion for fatigue", *Nucl. Eng. Des.,* **3**, 32-40.
Sumi, Y., Mohri, M. and Kawamura, Y. (2005), "Computational prediction of fatigue crack paths in ship structural details", *Fatigue Fract. Eng. M.,* **28**(1-2), 107-115.
Tarar, W. (2008), "A new finite element procedure for fatigue life prediction and high strain rate assessment of AHSS", PhD Dissertation, The Ohio State University.
Tarar, W., Scott-Emuakpor, O. and Shen, M.H. (2007), "A new finite element for gas turbine engine fatigue life prediction", *Proceedings of ASME/IGTI Turbo Expo*, GT2007-27427.